


Cite this: *RSC Adv.*, 2022, 12, 35959

# Co<sub>3</sub>O<sub>4</sub>@chitosan/La<sub>2</sub>O<sub>3</sub> nanocomposites as innovative, powerful, and recyclable nanocatalysts for sonochemical treatment of benzyl alcohols to obtain the corresponding benzaldehyde derivatives†

Fereshteh Javidfar,<sup>a</sup> Manoochehr Fadaeian<sup>\*a</sup> and Javad Safaei Ghomi<sup>ab</sup>

Ultrasonic (US) irradiation (100 W, 40 kHz) reactions, used as a safe and green technique, are often more efficient than traditional protocols. This leads us to introduce, for the first time, an efficient nanocatalyst and immobilization of La<sub>2</sub>O<sub>3</sub> nanoparticles on Co<sub>3</sub>O<sub>4</sub> nanoparticles for the selective oxidation of benzyl alcohol to the corresponding benzaldehyde at room temperature. The structural and morphological characteristics of the nanocatalysts were determined by FT-IR, XRD, FE-SEM, EDX, and VSM. The catalytic performance of the Co<sub>3</sub>O<sub>4</sub>@Cs/La<sub>2</sub>O<sub>3</sub> composites used as heterogeneous nanocatalysts was investigated in the selective oxidation of benzylic alcohols to their corresponding benzaldehydes. Also, the performance of the oxidation parameters, including H<sub>2</sub>O<sub>2</sub> concentration, time, effect of various solvents, and nanocatalyst dosage was checked. Significant benefits of this method can be named by using a non-toxic solvent, easy product isolation, excellent recoverability, low time of reaction, high yield, and ultrasound irradiation. Finally, a possible mechanism was proposed to show the nanocatalytic process.

Received 17th August 2022  
Accepted 1st October 2022

DOI: 10.1039/d2ra05154k

rsc.li/rsc-advances

## 1. Introduction

One of the most challenging functional group transformations for good chemical production in both the laboratory and at industrial scale is considered to be the selective oxidation of benzyl alcohol to its corresponding benzaldehyde (BZD).<sup>1,2</sup> Generally, conventional inorganic and traditional oxidants such as Cr(vi) oxides, pyridinium chlorochromate (PCC), and permanganate (MnO<sub>4</sub><sup>−</sup>), and so on, are toxic, unstable, expensive, and hazardous to use.<sup>2</sup> Therefore, they produce a great amount of toxic waste, the recovery of which requires many extra chemical processes that are expensive and dangerous. Thus, it is not economically feasible and causes environmental danger. Therefore, from the perspective of green chemistry and being eco-friendly, the use of such oxidation should be avoided. Recently, environmental pollution has become one of the most important challenges, and for this reason, chemists are

choosing reactants, the reaction products of which cause the lowest pollution and hazards to the environment. So, hydrogen peroxide (H<sub>2</sub>O<sub>2</sub>) is a strong, green, cheap, mild, and ecofriendly oxidizer, and its only by-product is H<sub>2</sub>O. Thanks to its special and attractive properties, chemists have assigned a great amount of time to researching the uses of H<sub>2</sub>O<sub>2</sub>.<sup>6,7</sup>

In terms of quantity used, BZD (with a smell of bitter almonds) is the second most important aromatic molecule (after vanillin). In this field, the catalytic processes that lead to excellent-quality BZD are particularly appealing for use in the perfume and food industries, pharmaceuticals, dyes, beverages, agribusiness industries, and chemicals.<sup>3–7</sup>

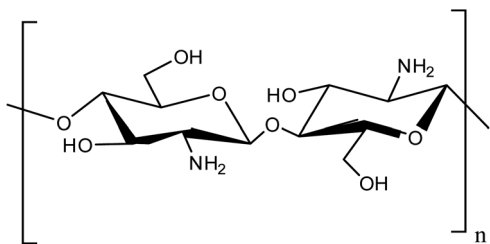
The most plentiful polysaccharide, other than cellulose, is chitin, which has many properties such as biodegradability and biocompatibility.<sup>8</sup> Chitosan (CS) is the basic derivative of chitin. Recently, CS has attracted the attention of chemists due to its abundant properties such as inexpensiveness, it is an abundant resource, hydrophilicity, environmentally friendliness, non-toxicity, excellent chemical and thermal stability, and its anti-fungal, antibacterial, and antioxidant properties. Also, the NH<sub>2</sub> and OH groups in the CS structure provide diverse coordination sites for chemical modifications such as chelating ligands to coordinate different metal ions to synthesize magnetic composites,<sup>7–12</sup> (Scheme 1).

<sup>a</sup>Department of Chemistry, Qom Branch, Islamic Azad University, Post Box: 37491-13191, Qom, Iran. E-mail: fadaeian\_m@yahoo.com; Fax: +98 9128236206; Tel: +98 2537780045

<sup>b</sup>Department of Organic Chemistry, Faculty of Chemistry, University of Kashan, Kashan, Iran

† Electronic supplementary information (ESI) available. See DOI: <https://doi.org/10.1039/d2ra05154k>





Scheme 1 Chitosan structure.

Recently, cobalt oxide ( $\text{Co}_3\text{O}_4$ ) nanoparticles (NPs) have become an important, magnetic, and well-known p-type semiconductor that has increasingly attracted attention because it is inexpensive and ecofriendly, is simple to prepare and has high chemical and physical stability. The  $\text{Co}_3\text{O}_4$  has been studied because it is a promising substance with a great number of applications in lithium-ion batteries, gas sensing, information storage, heterogeneous catalysis, optical devices, magnetic materials, and electrochromic devices.<sup>13–15</sup>  $\text{Co}_3\text{O}_4$  with valence of more than 3 is unstable in the normal environment. However, other cobalt oxide forms such as  $\text{Co}_2\text{O}_3$  and  $\text{CoO}$ , are more stable and have more advantages in industrial applications.<sup>16</sup>

Lanthanum oxide ( $\text{La}_2\text{O}_3$ ) one of the rare earth oxides, has been investigated as a catalyst in different reactions because of its unique properties (excellent paramagnetic sensitivity, saturated magnetism, constriction magnetic properties, large bandgap, and so on). It is also a good candidate for studies because of its significant applications in electronics, sensors, insulators, antimicrobial agents, biomedicine, and biocatalysts. Therefore,  $\text{La}_2\text{O}_3$  is an excellent choice for research on improving its catalytic activity.<sup>1,2,6,7,17–19</sup>

In addition, the ultrasound (US) irradiation method is an ecofriendly, safe, and cheap technology which is used as a versatile tool in a vast range of scientific and technological applications.<sup>20–22</sup> In contrast to normal thermal heating, US irradiation has many important benefits: improved efficiency, a significant reduction in reaction time, increased selectivity, it is inexpensive and easy to handle and use in various procedures, and the compounds show excellent purity. Additionally, in many cases, reactions under US irradiation could be considered as being ecofriendly procedures and use a small number of solvents.<sup>23,24</sup> Therefore, US irradiation causes the least number of side reactions.<sup>25</sup>

In this regard, a fast and green method for the synthesis of  $\text{Co}_3\text{O}_4@\text{Cs}/\text{La}_2\text{O}_3$  nanocomposites for use as novel heterogeneous nanocatalysts is proposed and its efficiency in the oxidation of benzyl alcohol to BZD is also explored. We developed the oxidation of benzyl alcohol to BZD at room temperature and under US conditions. As understood from this proposed procedure, it greatly complements the goals of green chemistry, and it can be used effectively in the production of BZD, with the use of the  $\text{Co}_3\text{O}_4@\text{Cs}/\text{La}_2\text{O}_3$  nanocomposites as a nanocatalyst. It also shows massive advantages for both use in industry and academia.

## 2. Results and discussion

The Fourier transform infrared (FT-IR) spectrum of  $\text{Co}_3\text{O}_4@\text{Cs}/\text{La}_2\text{O}_3$ ,  $\text{Co}_3\text{O}_4$ , and pure CS are shown in Fig. 1. The two strong absorbance bands at about 561 and 660  $\text{cm}^{-1}$  (565 and 661  $\text{cm}^{-1}$ ) were ascribed to the Co–O stretching vibrations (Fig. 1a and c).<sup>16,26</sup> The absorption bands at 3364, and 3434  $\text{cm}^{-1}$  were ascribed to the amino and hydroxyl groups of CS, and also the bands at 1384 and 1374  $\text{cm}^{-1}$  were related to the C–O stretching vibration of the hydroxyl groups of CS. The bands at 1649 and 1635  $\text{cm}^{-1}$  corresponded to the C=O stretching vibration of the amide group (Fig. 1b and c).<sup>27–30</sup> The characteristic bands at 419  $\text{cm}^{-1}$  were due to the La–O stretching band (Fig. 1c).<sup>6,7,31</sup>

In the energy-dispersive X-ray spectroscopy (EDX) spectrum shown in Fig. 2, the presence of the elements: C, Co, La, N, and O, was determined according to their energy, which indicated the confirmation of the product purity.

Data obtained from the X-ray diffraction (XRD) analysis, which was used in analysis of the  $\text{Co}_3\text{O}_4@\text{Cs}/\text{La}_2\text{O}_3$  catalyst synthesized in this project, is shown in Fig. 3. The XRD samples for  $\text{Co}_3\text{O}_4$ , CS,  $\text{La}_2\text{O}_3$  NPs, and the  $\text{Co}_3\text{O}_4@\text{Cs}/\text{La}_2\text{O}_3$  nanocomposite are shown in Fig. 3a–d. The developed peaks indicate the dimensions of the nano sized particles. The characteristic peaks for  $\text{Co}_3\text{O}_4$  are found in the region at  $2\theta$  of 31.3°, 36.89°, 44.83°, 55.61°, 59.43°, and 65.42°, which corresponded to (220), (311), (400), (422), (511), and (440), respectively. The network parameters agreed well with those of the JCPDS card number 01-078-1969 (standard cubic  $\text{Co}_3\text{O}_4$ ).<sup>32</sup> The broad diffraction peaks of CS show  $2\theta = 10.60$  and 19.9° and it was a good match with the results given in past reports.<sup>6,33</sup> Also, the  $\text{La}_2\text{O}_3$  NPs had peaks that are shown at 27.2912°, 28.3643°, 39.6213°, and 46.4585° and are related to  $\text{La}_2\text{O}_3$ , which correspond to (222), (300), (400), and (622), respectively, ( $\text{La}_2\text{O}_3$ , JCPDS card no. 04-0856).<sup>34</sup> Characteristic peaks for  $\text{Co}_3\text{O}_4$  and  $\text{La}_2\text{O}_3$  indicated that the structure of them both had not changed during the combination process.

Scanning electron microscopy (SEM) is a powerful technique for investigating surface morphology. The morphology,

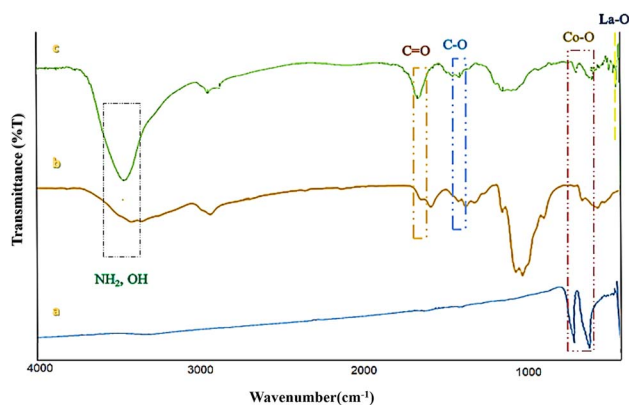
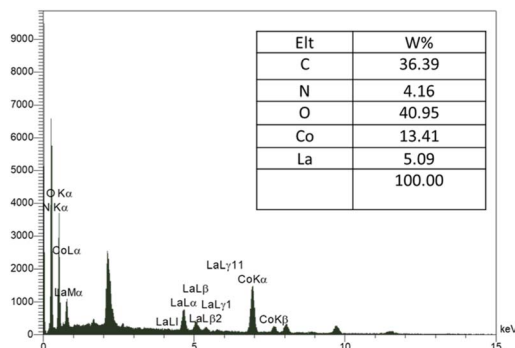
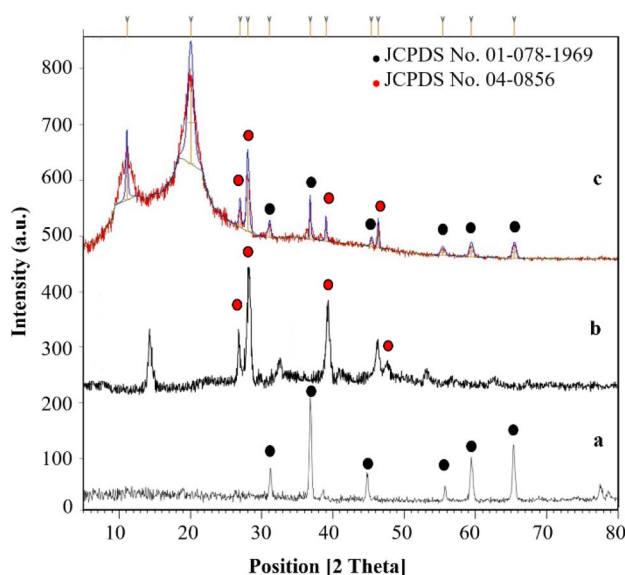


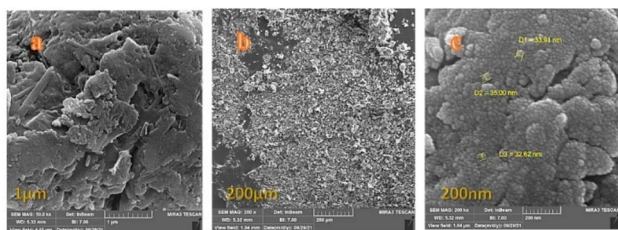
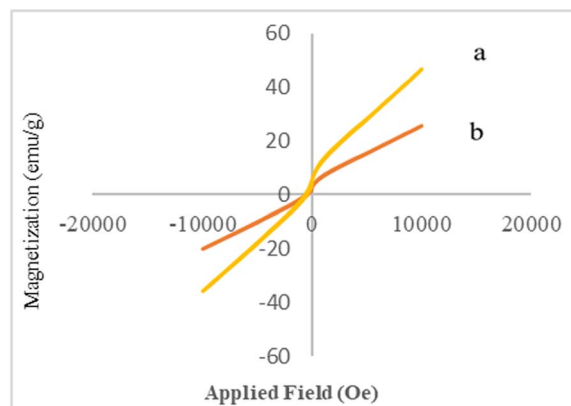
Fig. 1 The FT-IR spectra of (a)  $\text{Co}_3\text{O}_4$ , (b) pure CS, and (c)  $\text{Co}_3\text{O}_4@\text{Cs}/\text{La}_2\text{O}_3$  nanocomposites.



Fig. 2 The EDX spectrum of  $\text{Co}_3\text{O}_4@\text{Cs}/\text{La}_2\text{O}_3$ .Fig. 3 The XRD patterns of (a)  $\text{Co}_3\text{O}_4$ , (b) CS, and (c)  $\text{La}_2\text{O}_3$  and  $\text{Co}_3\text{O}_4@\text{Cs}/\text{La}_2\text{O}_3$ .

size, and form of the catalyst were surveyed by SEM at different magnifications. The result was that the FE-SEM images showed a magnetic  $\text{Co}_3\text{O}_4@\text{Cs}/\text{La}_2\text{O}_3$  nanocomposite consisting of nearly spherical particles with a size of about 32–35 nm (Fig. 4).

The magnetic behaviors of  $\text{Co}_3\text{O}_4$  and  $\text{Co}_3\text{O}_4@\text{Cs}/\text{La}_2\text{O}_3$  were determined using a vibrating sample magnetometer (VSM) at room temperature (Fig. 5). There was no hysteresis,

Fig. 4 The FE-SEM images, at different magnifications, of the  $\text{Co}_3\text{O}_4@\text{Cs}/\text{La}_2\text{O}_3$  catalyst, (a) 1  $\mu\text{m}$ , (b) 200  $\mu\text{m}$ , and (c) 2000 nm.Fig. 5 The VSM results, (a)  $\text{Co}_3\text{O}_4$ , and (b)  $\text{Co}_3\text{O}_4@\text{Cs}/\text{La}_2\text{O}_3$  nanocomposites.


coercivity, or remanence in bare  $\text{Co}_3\text{O}_4$  and  $\text{Co}_3\text{O}_4@\text{Cs}/\text{La}_2\text{O}_3$  samples at room temperature, which showed their typical superparamagnetic behavior. The  $\text{Co}_3\text{O}_4$  NPs and  $\text{Co}_3\text{O}_4@\text{Cs}/\text{La}_2\text{O}_3$  had superparamagnetic behavior, which facilitated the magnetic separation. The saturation magnetization values ( $M_s$ ) of the  $\text{Co}_3\text{O}_4$  NPs and  $\text{Co}_3\text{O}_4@\text{Cs}/\text{La}_2\text{O}_3$  nanocomposites were 46.5 and 25.8  $\text{emu g}^{-1}$ , respectively. However, the addition of the CS layer and the  $\text{La}_2\text{O}_3$  NPs on the  $\text{Co}_3\text{O}_4$  surface results decreased the magnetic behavior, and the  $\text{Co}_3\text{O}_4@\text{Cs}/\text{La}_2\text{O}_3$  nanocomposite saturation magnetization was sufficient for a rapid magnetic separation by an external magnet.<sup>7,35</sup>

## 2.1. Catalytic activity of $\text{Co}_3\text{O}_4@\text{Cs}/\text{La}_2\text{O}_3$ nanocomposites

The catalytic activity of the  $\text{Co}_3\text{O}_4@\text{Cs}/\text{La}_2\text{O}_3$  was compared with that of various catalysts to determine the requirement for the presence of a catalyst for the oxidation of benzyl alcohols (Table 1). The oxidation of benzyl alcohols to the corresponding BZDs was performed under a mild reaction and sonochemical conditions. Oxidation under sonication conditions plays a fundamental role in this process. Also, the benzyl alcohols were oxidized both in the presence of, and without the  $\text{Co}_3\text{O}_4@\text{Cs}/\text{La}_2\text{O}_3$  nanocatalyst (Table 1, entries 5–8). The yield of BZD obtained was established to be only 58%, 63%, 80%, 85%, and 97% in the presence of 50 mg of  $\text{Co}_3\text{O}_4@\text{Cs}/\text{La}_2\text{O}_3$  and different solvents (Table 1, entries 1–5), respectively. The oxidation of benzyl alcohol was carried out using 50 mg of  $\text{Co}_3\text{O}_4@\text{Cs}/\text{La}_2\text{O}_3$  without any solvent. Also, the yield of BZD formation without a catalyst was decreased (Table 1, entry 8). When the catalyst amount was increased, the BZD was obtained with a lower yield (Table 1, entry 9). In Table 1, a large comparison of the catalytic activities of  $\text{Co}_3\text{O}_4@\text{Cs}/\text{La}_2\text{O}_3$  with other catalysts used in the oxidation of benzyl alcohol is shown (Table 1, entries 12–20). It was concluded, that the catalyst gave excellent results and offered very gentle reactions conditions and was a green option.

Table 2 summarizes the results from the  $\text{Co}_3\text{O}_4@\text{Cs}/\text{La}_2\text{O}_3$  nanocatalyst oxidation reactions. A wide range of aromatic alcohols has been changed to benzaldehyde



Table 1 The effect of different conditions on the benzyl alcohol oxidation<sup>a</sup>


Entry	Catalyst <sup>Ref</sup>	Catalyst (mg)	Time (min)	Temperature (°C)	Oxidant	Solvent	Yield <sup>b</sup> (%)
1	Co <sub>3</sub> O <sub>4</sub> @Cs/La <sub>2</sub> O <sub>3</sub>	50	15	r.t./US	H <sub>2</sub> O <sub>2</sub>	<i>m</i> -Xylene	58
2	Co <sub>3</sub> O <sub>4</sub> @Cs/La <sub>2</sub> O <sub>3</sub>	50	15	r.t./US	H <sub>2</sub> O <sub>2</sub>	Toluene	63
3	Co <sub>3</sub> O <sub>4</sub> @Cs/La <sub>2</sub> O <sub>3</sub>	50	15	r.t./US	H <sub>2</sub> O <sub>2</sub>	CH <sub>3</sub> CN	80
4	Co <sub>3</sub> O <sub>4</sub> @Cs/La <sub>2</sub> O <sub>3</sub>	50	15	r.t./US	H <sub>2</sub> O <sub>2</sub>	Ethanol	85
5	Co <sub>3</sub> O <sub>4</sub> @Cs/La <sub>2</sub> O <sub>3</sub>	50	8	r.t./US	H <sub>2</sub> O <sub>2</sub>	Free solvent	97
6	Co <sub>3</sub> O <sub>4</sub> @Cs	50	8	r.t./US	H <sub>2</sub> O <sub>2</sub>	Free solvent	84
7	Co <sub>3</sub> O <sub>4</sub>	50	8	r.t./US	H <sub>2</sub> O <sub>2</sub>	Free solvent	73
8	Null	—	15	r.t./US	H <sub>2</sub> O <sub>2</sub>	Free solvent	50
9	Co <sub>3</sub> O <sub>4</sub> @Cs/La <sub>2</sub> O <sub>3</sub>	75	10	r.t./US	H <sub>2</sub> O <sub>2</sub>	Free solvent	86
10	Co <sub>3</sub> O <sub>4</sub> @Cs/La <sub>2</sub> O <sub>3</sub>	50	180	130	H <sub>2</sub> O <sub>2</sub>	<i>m</i> -Xylene	87
11	Co <sub>3</sub> O <sub>4</sub> @Cs/La <sub>2</sub> O <sub>3</sub>	50	160	130	H <sub>2</sub> O <sub>2</sub>	Ethanol	88
12	Co <sub>3</sub> O <sub>4</sub> @Cs/La <sub>2</sub> O <sub>3</sub>	50	300	130	H <sub>2</sub> O <sub>2</sub>	CH <sub>3</sub> CN	87
13	Null	—	240	130	H <sub>2</sub> O <sub>2</sub>	<i>m</i> -Xylene	91
14	ZPCu <sup>37</sup>	0.005	60	90	H <sub>2</sub> O <sub>2</sub>	Free solvent	90
15	Au-Pd/C <sup>39</sup>	2	240	80	H <sub>2</sub> O <sub>2</sub>	Free solvent	11.32
16	ZnBr <sub>2</sub> (ref. 40)	0.02	90	Reflux	Chloramine-T	CH <sub>3</sub> CN	96
17	Au/Al <sub>2</sub> O <sub>3</sub> (ref. 41)	48	15	100	O <sub>2</sub>	Toluene	86
18	(TEAH)H <sub>2</sub> PW <sub>12</sub> O <sub>40</sub> (ref. 42)	0.04	180	100	H <sub>2</sub> O <sub>2</sub>	H <sub>2</sub> O	99.6
19	FSPC <sup>43</sup>	50	15	r.t.	H <sub>2</sub> O <sub>2</sub>	CH <sub>3</sub> CN	70
20	WO <sub>4</sub> @PMO-IL <sup>44</sup>	0.0015	720	90	H <sub>2</sub> O <sub>2</sub>	CH <sub>3</sub> CN : H <sub>2</sub> O	75

<sup>a</sup> Reaction conditions: benzyl alcohols (1 mmol), H<sub>2</sub>O<sub>2</sub> (1 ml), Co<sub>3</sub>O<sub>4</sub>@Cs/La<sub>2</sub>O<sub>3</sub> (0.05 g). <sup>b</sup> Isolated yield.

derivatives with great yields within a short reaction time at room temperature (Table 2). Both electron-donating and electron-withdrawing groups accelerated the oxidation reaction, but the presence of any steric hindrance around the hydroxyl group of the benzyl alcohol substituent at the *ortho* or *meta* position caused decreased yields and a longer reaction time (Table 2, entries 1, 4, 6, 8, 9 and 11). However, when compared with the *para* position, because of the absence of steric hindrance, there was an increase in the yield and a decrease in time.<sup>6,36,37</sup>

According to all this information and the investigation, an acceptable mechanism for this oxidation was proposed. The results demonstrated that La<sup>3+</sup> (on the surface of Co<sub>3</sub>O<sub>4</sub>@Cs/La<sub>2</sub>O<sub>3</sub>) acts as a Lewis acid site in the oxidation of benzyl alcohols. The La<sup>3+</sup> was coordinated to the oxygen of the peroxide hydrogen and formed an La-OOH intermediate A as the first step. In the second step, intermediate A reacted with benzyl alcohols to form intermediate B, and the deletion of an H<sub>2</sub>O molecule from intermediate B, resulted in intermediate C, and at the end, it resulted in the elimination of the secondary H<sub>2</sub>O molecule and created the corresponding BZD (Scheme 2).<sup>6,36–38</sup>

## 2.2. Catalyst reutilization

For catalytic activity, stability plays an essential role. In this project, the catalyst reusability of the Co<sub>3</sub>O<sub>4</sub>@Cs/La<sub>2</sub>O<sub>3</sub> was investigated under optimum reaction conditions. The results showed that the Co<sub>3</sub>O<sub>4</sub>@Cs/La<sub>2</sub>O<sub>3</sub> was recovered up to the fifth cycle (Fig. 6). The results of the XRD analysis of the Co<sub>3</sub>O<sub>4</sub>@Cs/La<sub>2</sub>O<sub>3</sub> nanocatalysts after five cycles of reuse are shown in Fig. 7b. The characteristic peaks for Co<sub>3</sub>O<sub>4</sub>@Cs/La<sub>2</sub>O<sub>3</sub> were conserved, showing that the nanocatalysts had been very stable and pure.

## 3. Experimental

### 3.1. Chemicals and apparatus

For this work, all the high quality material and chemicals, including alcohol and solvents needed for the experiments, were purchased from Merck and the Aldrich Company. The FT-IR spectroscopy samples were dispersed in KBr and then made into pellets and their spectra were acquired using a PerkinElmer 1600 FTIR spectrometer. In addition, the morphology and size of the samples were determined by SEM, and the crystals were investigated by XRD, EDX, and VSM. The oxidation yields were investigated using gas chromatographic spectrometry (GC).





Table 2 Oxidation of benzyl alcohols to benzyl aldehydes<sup>a</sup>

Entry	X	Time (min)	Yield <sup>b</sup> (%)	Selectivity (%)
1	3-Hydroxy	10	87	>99
2	4-Hydroxy	8	97	>99
3	4-Chloro	8	97	>99
4	2-Chloro	10	83	>99
5	4-Methoxy	8	96	>99
6	3-Methoxy	10	90	>99
7	4-Methyl	8	97	>99
8	3-Methyl	10	92	>99
9	3-iPr	12	87	>99
10	4-Nitro	8	96	>99
11	3-Nitro	10	87	>99
12	4-Fluoro	8	95	>99
13	4-Bromo	8	96	>99
14	3-Bromo	10	83	>99
15	Benzyl alcohol	8	97	>99

<sup>a</sup> Reaction conditions: benzyl alcohols (1 mmol), H<sub>2</sub>O<sub>2</sub> (1 ml), Co<sub>3</sub>O<sub>4</sub>@CS/La<sub>2</sub>O<sub>3</sub> (0.05 g). <sup>b</sup> Isolated yield.

### 3.2. Preparation of the Co<sub>3</sub>O<sub>4</sub> nanoparticles

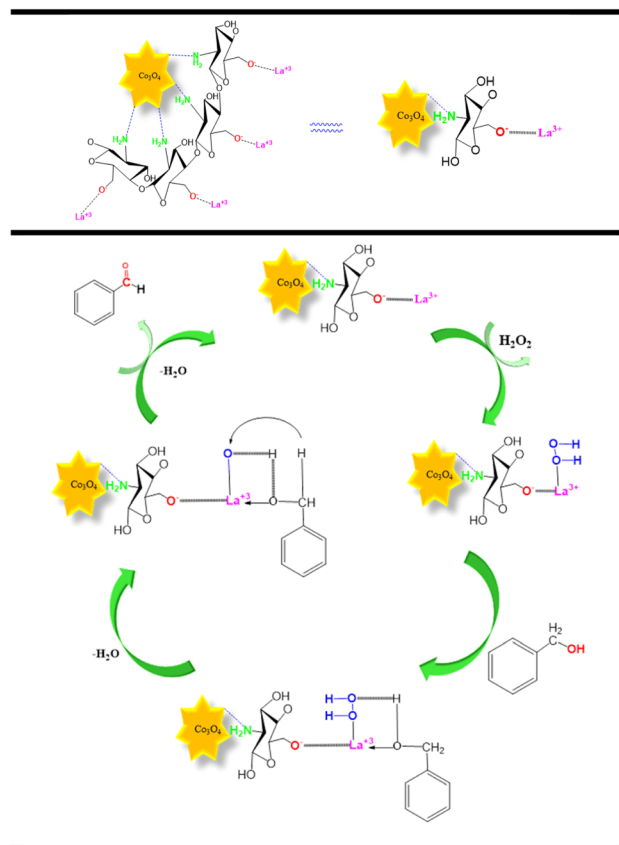
The Co<sub>3</sub>O<sub>4</sub> NPs were fabricated according to method found in the literature and were obtained successfully. Approximately 8.60 g of cobalt(II) nitrate was dissolved in 100 ml of EtOH for about 30 s, in a round bottomed flask. Then, 2.14 g of ethanedioic acid was slowly added and the reaction mixture was stirred for 2 h at 45 °C. The precipitate formed consisted of cobalt(II) oxalate powder and was collected by centrifugation followed by calcining at 400 °C for 2 h to produce the Co<sub>3</sub>O<sub>4</sub> NPs.<sup>45</sup>

### 3.3. Preparation of Co<sub>3</sub>O<sub>4</sub>@CS

The Co<sub>3</sub>O<sub>4</sub>@Cs nanocomposites were synthesized according to our previous method.<sup>7</sup> The Co<sub>3</sub>O<sub>4</sub>@CS nanocomposites were prepared by dispersing 0.01 g CS dissolved in 10 ml of ethanoic acid. Next, 0.25 g of Co<sub>3</sub>O<sub>4</sub> was added to the CS solution and dispersed for 30 min. The reaction mixture was mechanically stirred at 60 °C. Subsequently, a solution was made by dissolving 0.02 g of sodium tripolyphosphate (STPP) in 50 ml of deionized water, which was added dropwise at a rate of 4.5 ml h<sup>-1</sup>. At this step, the ionic gelation of CS occurred on the Co<sub>3</sub>O<sub>4</sub> MNP surface. Next, after filtration, the reaction mixture was dried for 36 h at -20 °C. Finally, the core-shell product of the Co<sub>3</sub>O<sub>4</sub>@Cs NPs was obtained.

### 3.4. Procedure for the preparation of Co<sub>3</sub>O<sub>4</sub>@Cs/La<sub>2</sub>O<sub>3</sub>

The Co<sub>3</sub>O<sub>4</sub>@Cs/La<sub>2</sub>O<sub>3</sub> nanocomposites were prepared according to our previous method.<sup>6,7</sup> The Co<sub>3</sub>O<sub>4</sub>@Cs/La<sub>2</sub>O<sub>3</sub>



Scheme 2 A possible reaction mechanism.

nanocomposites were created by dispersing about 0.1 g of Co<sub>3</sub>O<sub>4</sub>@Cs in deionized water (50 ml) and sonicating the mixture for 60 min. Subsequently, 0.05 g of LaCl<sub>3</sub>·7H<sub>2</sub>O was added. The reaction mixture was stirred for about 120 min under reflux conditions. Finally, the products were separated by centrifugation, and then washed three times with distilled water.

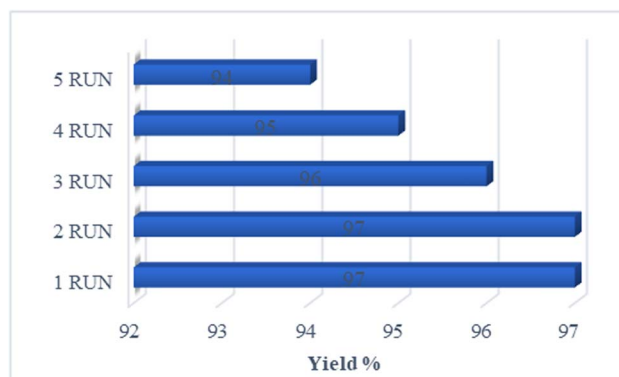


Fig. 6 Recyclability of the sonocatalyst.



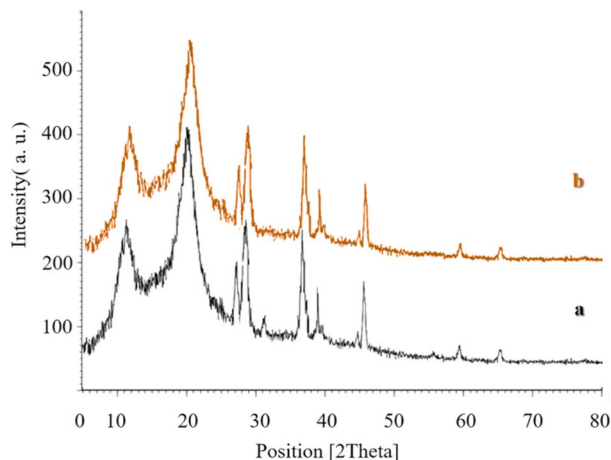


Fig. 7 Comparison of the XRD spectra of the prepared  $\text{Co}_3\text{O}_4@\text{Cs}/\text{La}_2\text{O}_3$  (a) before, and (b) after five runs.

### 3.5. General procedure for the oxidation of benzyl alcohols

A mixture of benzyl alcohol (1 mmol),  $\text{H}_2\text{O}_2$  (1 ml) and  $\text{Co}_3\text{O}_4@\text{Cs}/\text{La}_2\text{O}_3$  (0.05 g) was added to a round bottomed flask and the mixture was sonicated in an ultrasonic bath (constant frequency) at 25 °C. After the completion of the oxidation, as determined out by thin-layer chromatography (TLC), the magnetic catalyst was separated using an external magnet.<sup>7</sup>

## 4. Conclusions

In conclusion, we designed and investigated  $\text{Co}_3\text{O}_4@\text{Cs}/\text{La}_2\text{O}_3$  nanocatalysts. Also, the oxidation of benzyl alcohol derivatives to different benzaldehydes using the  $\text{Co}_3\text{O}_4@\text{Cs}/\text{La}_2\text{O}_3$  nanocatalysts was carried out at room temperature under ultrasonic irradiation conditions. Using the previously mentioned conditions, the catalytic activity of nanocatalysts for the selective oxidation of benzyl alcohols to benzaldehyde was investigated (Table 2). The benzyl alcohol derivatives were oxidized to the corresponding benzaldehyde, with excellent yield, within 8 min. Benzaldehydes are known to be significant intermediates, which are oxidized by benzyl alcohol in industry and chemistry. Therefore, the mechanism of the oxidation of benzyl alcohol is of particular importance for organic chemists. Some of the properties of the  $\text{Co}_3\text{O}_4@\text{Cs}/\text{La}_2\text{O}_3$  nanocatalysts include a decreased reaction time, the ability to be easily separated magnetically, the retention of excellent chemical stability after five periods of reuse, increased selectivity, and high yield.

## Conflicts of interest

The authors state that they had no financial or personal conflicts of interest in preparing the materials reported in this article.

## References

- J. Yang, K. Cao, M. Gong, B. Shan and R. Chen, *J. Catal.*, 2020, **386**, 60–69.
- T. Tamiji and A. Nezamzadeh-Ejhieh, *Mater. Chem. Phys.*, 2019, **12**, 121813.
- R. Hudson, Y. Feng, R. S. Varma and A. Moores, *Green Chem.*, 2014, **16**, 4493–4505.
- J. C. Colmenares, W. Ouyang, M. Ojeda, E. Kuna, O. Chernyayeva, D. Lisovtyskiy, S. De, R. Luque and A. M. Balu, *Appl. Catal., B*, 2015, **183**, 107–112.
- M. J. Jacinto, P. K. Kiyohara, S. H. Masunaga, R. F. Jardim and L. M. Rossi, *Appl. Catal., A*, 2008, **338**, 52–57.
- F. Javidfar, M. Fadaeian and J. Safaei Ghomi, *Polycyclic Aromat. Compd.*, 2021, 1–11.
- F. Javidfar, M. Fadaeian and J. Safaei Ghomi, *RSC Adv.*, 2021, **11**, 35988–35993.
- M. Nasrollahzadeh, N. Shafiei, Z. Nezafat, N. Sadat Soheili Bidgoli and F. Soleimani, *Carbohydr. Polym.*, 2020, **241**, 116253.
- J. Safari, F. Azizi and M. Sadeghi, *New J. Chem.*, 2015, **39**, 1905–1909.
- J. Safari and Z. Zarnegar, *RSC Adv.*, 2014, **4**, 20932–20939.
- Y. Xie, X. Liu and Q. Chen, *Carbohydr. Polym.*, 2007, **69**, 142–147.
- D. H. K. Reddy and S. M. Lee, *Adv. Colloid Interface Sci.*, 2013, **68**, 201–202.
- A. B. Vennela, D. Mangalaraj, N. Muthukumarasamy, S. Agilan and K. V. Hemalatha, *Int. J. Electrochem. Sci.*, 2019, **14**, 3535–3552.
- T. O. Ahmadova, Z. Durmusa, A. Baykala and H. Kavasb, *Inorg. Mater.*, 2011, **47**, 426–430.
- C. Ramamoorthy and V. Rajendran, *Optik*, 2017, **145**, 330–335.
- S. A. Makhlof, *et al.*, *Superlattices Microstruct.*, 2013, **64**, 107–177.
- H. Dabhane, S. Ghotekar, P. Tambade and V. Medhane, *Asian. J. Nano. Mat.*, 2020, **3**, 291–299.
- X. Long, L. He, W. Ye and Q. Sun, *J. Electron. Mater.*, 2020, **49**, 6611–6621.
- C. Jin, Q. Yao, J. Li, B. Fan and Q. Sun, *Mater. Des.*, 2015, **15**, 205–210.
- J. A. Fuentes-García, J. Santoyo-Salzar, E. Rangel-Cortes, G. F. Goya, V. Cardozo-Mata and J. A. Pescador-Rojas, *Ultrason. Sonochem.*, 2020, 105274.
- J. Wang, J. Fan, J. Li, X. Wu and G. Zhang, *Ultrason. Sonochem.*, 2018, **48**, 404–411.
- E. A. Dil, M. Ghaedi, A. Asfaram, F. Zare, F. Mehrabi and F. Sadeghfhar, *Ultrason. Sonochem.*, 2017, **39**, 374–383.
- G. Zbancioc, O. Florea, P. Jones and I. I. Mangalagiu, *Ultrason. Sonochem.*, 2012, **19**, 399–403.
- M. Nikpassand, L. Z. Fekri and P. Farokhian, *Ultrason. Sonochem.*, 2016, **28**, 341–345.
- J. P. Hallett and T. Welton, *Chem. Rev.*, 2011, **111**, 3508–3576.
- M. Salavati-Niasari and A. Khansari, *C. R. Chim.*, 2014, **17**, 352–358.
- J. Safari and L. Javadian, *RSC Adv.*, 2014, **4**, 48973–48979.
- J. Safari and L. Javadian, *Ultrason. Sonochem.*, 2015, **22**, 341–348.
- J. Safari, F. Azizi and M. Sadeghi, *New J. Chem.*, 2015, **39**, 1905–1909.



- 30 J. Safari and Z. Zarnegar, *RSC Adv.*, 2014, **4**, 20932–20939.
- 31 N. Sulaiman, Y. Yulizar and D. O. B. Apriandanu, *AIP Conf. Proc.*, 2017, 020105.
- 32 U. Aftab, A. Tahira, A. Gradone, V. Morandi, M. I. Abro, M. M. Baloch and Z. H. Ibupoto, *Int. J. Hydrogen Energy*, 2021, **46**, 9110–9122.
- 33 M. Jiang, *et al.*, *Int. J. Biol. Macromol.*, 2010, **47**, 696–699.
- 34 P. Hou, C. Shi, L. Wu and X. Hou, *Microchem. J.*, 2016, **128**, 218–225.
- 35 A. A. Pathan, K. R. Desai and C. P. Bhasin, *Int. J. Nano. Chem.*, 2017, **3**, 21–25.
- 36 A. R. Hajipour, H. Karimi and A. Koohi, *Chin. J. Catal.*, 2015, **36**(7), 1109–1116.
- 37 A. R. Hajipour and H. Karimi, *Chin. J. Catal.*, 2014, **35**(9), 1529–1533.
- 38 L. Laasri, M. El Makhfi and S. Sebti, *Mater. Today.*, 2020, **31**, S156–S161.
- 39 S. Tareq, Y. H. T. Yap, T. A. Saleh, A. H. Abdul Halim Abdullah, U. Rashid and S. M. Izham, *J. Mol. Liq.*, 2018, **271**, 885–891.
- 40 P. Wang, J. Cai, J. Yang, C. Sun, L. Li, H. Hu and M. Ji, *Tetrahedron Lett.*, 2013, **54**, 533–535.
- 41 S. Rautiainen, O. Simakova, H. Guo, A.-R. Leino, K. Kordás, D. Murzin and D. T. Repo, *Appl. Catal., A*, 2014, **485**, 202–206.
- 42 H. Su and C. Yang, *Chin. J. Catal.*, 2014, **35**, 1224–1234.
- 43 S. Farhadi, Z. Babazadeh and M. Maleki, *Acta Chim. Slov.*, 2006, **53**, 72–76.
- 44 B. Karimi, F. B. Rostami, M. Khorasani, D. Elhamifar and H. Vali, *Tetrahedron*, 2014, **70**, 6114–6119.
- 45 C. C. Lin, Y. Guo and J. Vela, *ACS Catal.*, 2015, **5**, 51037–51044.

